ACS APPLIED MATERIALS & INTERFACES

Research Article

www.acsami.org

Three Dimensional Design of Large-Scale TiO_2 Nanorods Scaffold Decorated by Silver Nanoparticles as SERS Sensor for Ultrasensitive Malachite Green Detection

En-Zhong Tan,[†,‡] Peng-Gang Yin,*[,†] Ting-ting You,[†] Hua Wang,[†] and Lin Guo*[,†]

[†]Key Laboratory of Bio-Inspired Smart Interfacial Science and Technology of the Ministry of Education, School of Chemistry and Environment, Beihang University, Beijing 100191, PR China

[‡]Department of Mathematics and Physics, Beijing Institute of Technology Petrochemical, Beijing, 102617, PR China

Supporting Information

ABSTRACT: We have designed a large-scale three-dimensional (3D) hybrid nanostructure as surface-enhanced Raman scattering (SERS) sensor by decorating silver nanoparticles on TiO_2 nanorods scaffold (Ag/TiO_2). Taking *p*-mercaptobenzoic acid (PMBA) as the probe molecule, the SERS signals collected by point-to-point and time mapping modes show that the relative standard deviation (RSD) in the intensity of the main Raman vibration modes (1079, 1586 cm^{-1}) is less than 10%, demonstrating good spatial uniformity and time stability. This hybrid substrate also exhibits excellent SERS enhancement effect due to the formation of high-density hot spots among the AgNPs, which was proved by finite-difference time-domain (FDTD) simulations. The application of the new nanostructures as SERS sensors was demonstrated with the detection of malachite green (MG). The quantification of MG can be accomplished with the detection limit of 1×10^{-12} M based on the Raman intensity. The results show that the Ag/TiO_2 nanostructure can be a promising candidate for SERS sensor.

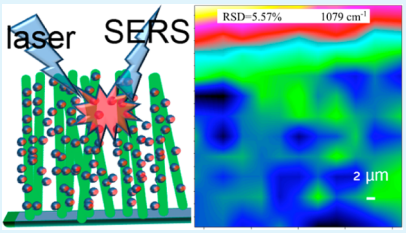

KEYWORDS: *surface-enhanced Raman scattering (SERS), TiO_2 nanorods scaffold, three dimension substrate, hot spot, malachite green*

1. INTRODUCTION

Surface-enhanced Raman scattering (SERS) is an ultrasensitive technique that enormously enhances Raman signals of molecules near the noble-metal nanostructures. SERS-based sensors have been applied in different kinds of domains due to their advantages in ultrasensitivity and ability to provide fingerlike structural information of analyte.[1−4] The main obstruction to the expansion of the scope of application for SERS sensors is the lack of large-scale SERS-active substrates with high-density hot spots yielding huge enhancement in a uniform way. Many researchers have been making substantive explorations in achieving qualified substrates. And different SERS substrates have been fabricated, including rough metal surface,[5,6] metal nanoparticles (NPs),[7] and well-ordered substrates.[8−13] Especially to the latter, various methods and techniques have been used to prepare ordered SERS substrates, such as self-assembly and Langmuir−Blodgett,[8−10] electron-beam lithography, nanosphere lithography, and nanoimprint lithography.[11−13] As we know, in the SERS effect, huge Raman enhancement arises on "hot spots" in metallic nanostructures owing to strong local electromagnetic fields coupling effect of adjacent metal nanostructures.[8,14−19] Nevertheless, the ordered substrates as mentioned above are mainly of two-dimensional (2D) distribution and the number of hot spots is quite limited.

Compared with 2D nanostructures, 3D nanostructures are far superior due to the fact that 3D spatial structures can supply more "hot spots" which provide giant enhancement. In addition, the 3D substrates can also supply larger surface area for adsorbing probe molecules than the 2D substrates. Therefore, they are more suitable for platform of SERS sensor. As-prepared highly sensitive 3D SERS substrates include different types of metal NPs decorating nanoporous semiconductors, such as silicon[20] and gallium nitride.[21] Another kind of well-defined 3D nanostructure used as the SERS substrates is anodic aluminum oxide with metal NPs.[22] In addition, a new family of 3D substrates with good repeatability and strong enhancement, nanorods arrays decorated with metal NPs, has come forth.[23−30] However, the presented 3D substrates have some drawbacks. For nanoporous semiconductors-based substrates, light propagation is limited owing to significant scattering and adsorption on pore walls and a significant fraction of closed pores, which decreases SERS enhancement.[20] And porous alumina membranes are fragile.[22] Hydrofluoric acid, an extremely hazardous acid, is required when silicon nanorods arrays are synthesized.[23,24,26] And ZnO arrays are unstable in strong acid and alkali solution.[27,28]

TiO_2 is one of the most important wide gap semiconductors, attracting extensive attention due to its outstanding optical and chemical properties.[31−34] TiO_2 nanoarray is a promising nanostructure because of its large surface area and/or high

Received: March 7, 2012
Accepted: June 18, 2012
Published: June 18, 2012

   dx.doi.org/10.1021/am3004126 | ACS Appl. Mater. Interfaces 2012, 4, 3432−3437

aspect ratio.[31−33] Recently, TiO_2 nanoarray has attracted intense interest as a potential candidate for fabrication of SERS substrates. As a result, a new kind of substrate with gold nanoparticles (AuNPs) supported on TiO_2 nanoarrays has been prepared; these hybrid structures are of high sensitivity, reproducibility, and uniformity.[29,35,36] It is well-known that AgNPs are materials with excellent SERS-activity and are much more cost-efficient in comparison with AuNPs. Therefore, it is a logical attempt to prepared Ag-modified TiO_2 nanoarray as SERS substrates. In this work, we prepared Ag/TiO_2 on fluorine-doped tin oxide (FTO) glass surface as SERS substrates in a simple method. The as-prepared Ag/TiO_2 composite is suitable for applying in real applications because of the chemical stability of TiO_2 and the physical stability of FTO. To evaluate the SERS activity of the as-prepared substrates, PMBA was used as the SERS probe molecule. The results show that Ag/TiO_2 composite is of high SERS-sensitivity due to more SERS hot sites arising from close-packed AgNPs in 3D space, which was well proved by FDTD simulations. In short, our presented hybrid nanostructures have great advantages as SERS sensors in practical applications: possessing a large-scale active area, excellent Raman enhancement, stability, and uniformity.

2. EXPERIMENTAL SECTION

Materials and Instruments. Titanium butoxide, glucose, MG, $AgNO_3$, HCl, and HNO_3 were of analytical grade and supplied by Beijing Reagent Company. PMBA was purchased from J&K Chemical Company and used as received without further purification. FTO substrates were supplied by Nippon Sheet Glass Group, Japan. Other reagents used in experiments were of analytical grade and used as received. The as-prepared substrates were characterized by Hitachi S-4800 scanning electron microscope (SEM) with 5.0 KV accelerating voltage. Transmission electron microscopy (TEM) and high-resolution TEM (HRTEM) images were received on a JEOL JEM-2100F microscope. Diffuse reflectance absorption spectra were obtained on a GBC Cintra 10e spectrometer with $BaSO_4$ as a reference. SERS measurements were approached on a JY HR800 Raman microscope with 647 nm as excitation and a 50× long distance objective and 600 lines/mm gratings (Note that the point-to-point mapping SERS spectra were obtained using a 10× objective).

TiO_2 Nanorods Scaffold Synthesis. Single-crystalline TiO_2 scaffold was synthesized according to the method provided in the literature.[31,32] In brief, 12 mL of deionized (DI) water was mixed with 12 mL of concentrated hydrochloric acid (36.5%−38% by weight) to reach a final volume of 24 mL. The mixture was poured into a Teflon-lined stainless steel autoclave and stirred under ambient conditions for 5 min, and then 0.4 mL of titanium butoxide was added. After another 5 min of stirring, one piece of cleaned FTO substrate was immersed into the solution. The autoclave was kept in an electric oven for 20 h at 150 °C, and then cooled to room temperature. Finally, the sample was taken out, rinsed extensively with DI water, and allowed to dry under ambient conditions.

Deposition of AgNPs on TiO_2 Nanorods Scaffold. The AgNPs were deposited on TiO_2 scaffold by an electroless deposition method, namely obtaining AgNPs by the reduction of $[Ag(NH_3)_2]^+$ with glucose. The preparation procedure is shown in Figure 1. For the preparation of $[Ag(NH_3)_2]^+$ solution, diluted ammonia solution was dropwise added to $AgNO_3$ solution until it became transparent, and the final concentration of Ag^+ was adjusted to 0.1 M. Subsequently, a piece of scaffold substrate was kept in this solution for several minutes followed by taking it out of the $[Ag(NH_3)_2]^+$ solution. Afterward, the substrate was dipped into DI water for several seconds and then immersed into a glucose solution for several minutes. After this process, the substrate was dipped once again into water to remove any glucose molecule. This decorating procedure was performed for several cycles to adapt the density and the size of the particles on the surface of the scaffold. We named the Ag/TiO_2 prepared by one, two, three, and four cycles as substrates A, B, C, and D, respectively.

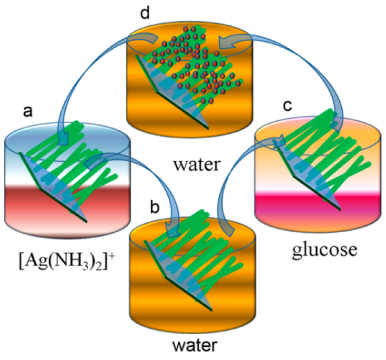

Figure 1. Scheme of decorating silver nanoparticles on TiO_2 nanorods scaffold.

3. RESULTS AND DISCUSSION

Morphologies of the As-prepared TiO_2 Scaffold and Substrates. SEM images were used to investigate the morphologies of the as-prepared TiO_2 scaffold and Ag/TiO_2 composite. Figure 2A shows the SEM image of TiO_2 NPs sheared off from TiO_2 scaffold and Figure 2B−2E show the SEM images of Ag/TiO_2 released from Ag decorated NRs scaffold. From the SEM images, we know that Ag coated the TiO_2 in the form of particles instead of film. Similar situations have been reported about metal NPs deposition on Si and ZnO nanoarrays.[23−28] NPs distributed on NRs in similar morphology with some variations in density and size (typically 10−30 nm). The density becomes higher and the average size grows bigger with the increase of number of decorating. Figure 2F shows a TEM image of a single Ag-modified NR removed from

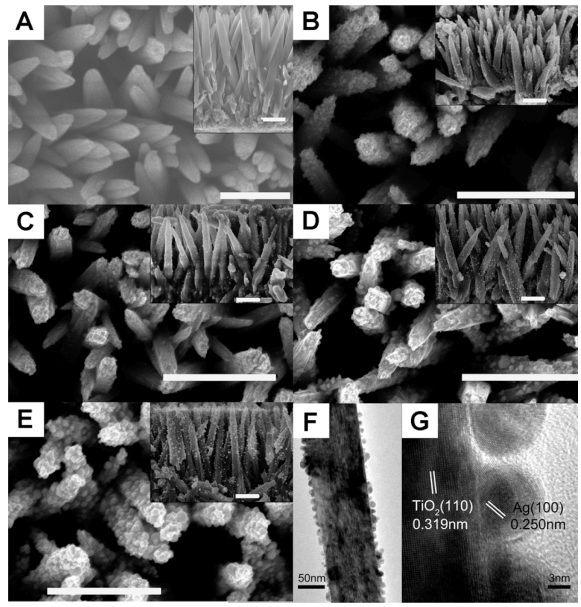

Figure 2. (A−E) SEM images of naked TiO_2 scaffold and Ag-modified scaffolds. (A) Naked TiO_2 scaffold; (B) substrate A; (C) substrate B; (D) substrate C; (E) substrate D; the insets are cross sections. Substrates A−D were prepared via depositing AgNPs on the scaffold by one, two, three, and four times. Scale bars: 500 nm. (F) TEM image of single Ag-modified TiO_2 NR removed from substrate D; (G) HRTEM image of the sample in image F.

the substrate D, while Figure 2G shows a high-resolution TEM (HRTEM) image of the detailed view of the Ag/TiO_2 composite in Figure 2F. The HRTEM image shows the crystalline quality of the TiO_2 NRs and AgNPs and also demonstrates that AgNPs were closely attached to the surface of the TiO_2.

Photos and Diffuse Reflectance Absorption Spectra of the As-Prepared TiO_2 Scaffold and Substrates. The photos and the corresponding diffuse reflectance absorption spectra of the as-prepared TiO_2 scaffold and substrates are shown in Figure 3. The TiO_2 scaffold can absorb only

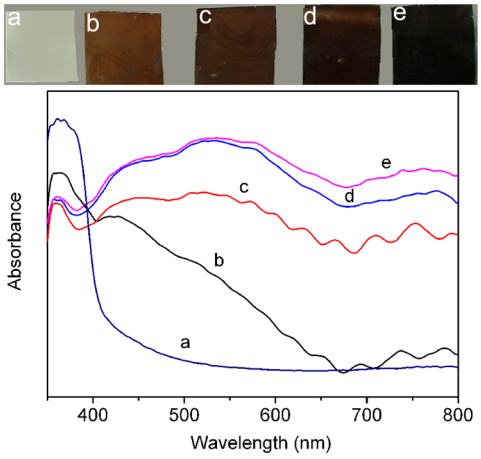

Figure 3. Photos (top) and corresponding diffuse reflectance absorption spectra (bottom) of the as-prepared TiO_2 scaffold and substrates: (a) TiO_2 scaffold; (b) substrate A; (c) substrate B; (d) substrate C; (e) substrate D. Substrates A–D were prepared via depositing AgNPs on TiO_2 scaffold one, two, three, and four times.

ultraviolet light with wavelength smaller than 410 nm. For Ag/TiO_2 substrates, the light absorbance extends to visible light region, and the strong absorption band is between 400 nm and 650 nm. The absorption wavelength of AgNPs with the size of 10–30 nm should be no more than 450 nm due to the localized surface plasmon resonance (LSPR) of Ag. In comparison with the absorption band of AgNPs in solution, the plasmon peak of as-prepared Ag/TiO_2 composite shows distinct broadening and redshift, which is attributed to a wide size distribution and interaction of the AgNPs.[37] In addition, the absorption spectra become stronger and more redshifted with the increase of AgNPs deposition times, which is actually because of the increased quantity and larger size of AgNPs. From the photos of the substrates, the color changes are also obvious. For the same reason, the color of Ag/TiO_2 substrates gets darker and darker with the longer deposition times. The result of X-ray diffraction patterns also show that AgNPs were adsorbed on TiO_2 scaffold after deposition (see Supporting Information).

SERS Property of the As-Prepared Substrates. To evaluate the SERS-activity of the as-prepared substrates, we selected PMBA as a probe molecule. PMBA is one of the most-used analytes in the SERS measurement and it has a distinct Raman feature. Studies have shown that PMBA is easy to adsorb on gold, silver, and copper surfaces to form a self-assembled monolayer.[34,35] The as-prepared substrates were immersed in 10^{-4} M PMBA ethanol solution for 30 min, in which the sufficient coverage of monolayer could be achieved on the Ag surface for estimation of the Raman enhancement factor (EF). After the PMBA adsorption, the substrates were thoroughly rinsed with ethanol to remove free molecules. The substrates were air-dried before acquiring the SERS spectra. The characteristic peaks of PMBA can be observed from Figure 4. We also measured the Raman spectrum of PMBA adsorbed

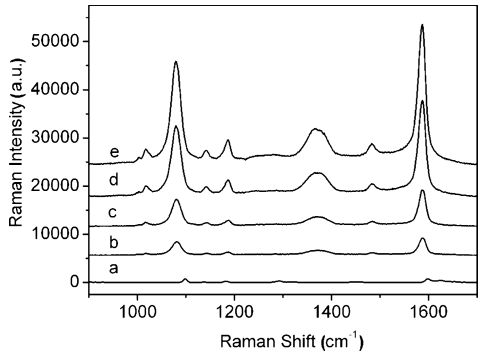

Figure 4. (a) Normal Raman spectrum of the solid PMBA. (b–e) SERS spectra of PMBA adsorbed on the substrates A, B, C, and D. Laser wavelength: 647 nm; power: 3mW; lens: 50× long distance objective; acquisition time: 2 s.

on the naked TiO_2 scaffold treated in the same way. No apparent Raman signal was found from that (spectrum not shown). The results confirmed that the enhancement of Raman signals of PMBA was attributed to the AgNPs.

As shown in Figure 4, the dominating characteristic bands of the normal Raman and SERS spectra of PMBA, ranging from 900 to 1700 cm^{-1}, are all observed clearly. According to previous studies, the predominant bands in the spectrum of solid PMBA are located at 1100, 1187, and 1596 cm^{-1}, which are assigned to a_1 modes of νCS, δCH, and νCC.[34,35] In SERS spectrum, the νCS band at 1100 cm^{-1} shifted to 1079 cm^{-1}, because of the formation of Ag–S bonding. The band νCC shifted from 1596 to 1586 cm^{-1}, and the δCH band shifted from 1187 to 1183 cm^{-1}. Band at 1079 cm^{-1} was selected as the representation for estimating the EF.

We estimated the average EF according to the following equation shown in the literature:[38–40]

$$\mathrm{EF} = \frac{I_{\mathrm{SERS}} N_{\mathrm{bulk}}}{I_{\mathrm{norm}} N_{\mathrm{surf}}}$$

where I_{SERS} and I_{norm} are the SERS and normal Raman intensities of the same peak, respectively, N_{bulk} and N_{surf} are the numbers of the probe molecules in the laser illumination volume in the bulk sample and on the SERS substrate, respectively (details can be found in Supporting Information). According to the account, EF was estimated to be 4.36×10^5 and it was high enough to ultrasensitive detection. In addition, more intense signals can be obtained compared to 2D substrates with the same EF due to more Ag nanoparticles and more hot spots in the probing zone. Similar enhancement phenomena were observed by other workers.[41]

To evaluate the uniformity of the as-prepared substrates, we collected the SERS spectra of PMBA by a 2D point by point mapping mode. The peaks mapped were 1079 and 1586 cm^{-1} and the strong SERS signals at each point demonstrated good reproducibility. As shown in Figure 5, on the 40 μm × 40 μm area, the values of RSD of the bands at 1079 and 1586 cm^{-1} are 5.57% and 4.94%, respectively. Furthermore, we verified the stability of the substrates by collecting the SERS spectra in the time-mapping mode. The results are illustrated in Figure 6, in

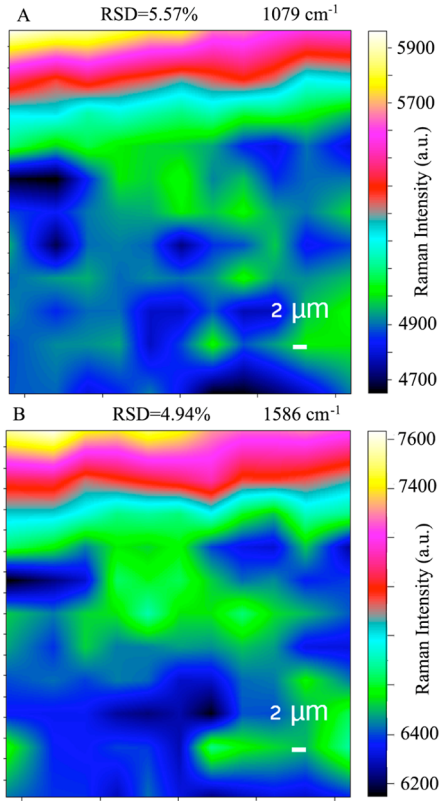

Figure 5. SERS mapping of the substrate D following PMBA adsorption, the peaks mapped were (A) 1079 cm^{-1} and (B) 1586 cm^{-1}. Laser wavelength: 647 nm; power: 10 mW; lens: 10× objective; acquisition time: 2 s.

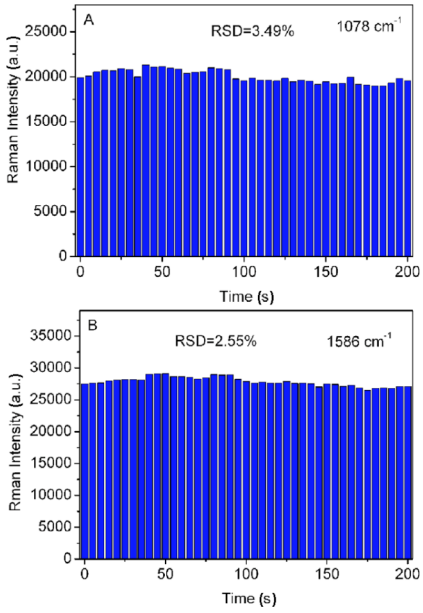

Figure 6. Intensities of SERS spectra of PMBA collected in the time-mapping mode on the substrate D, the peaks mapped were (A) 1079 cm^{-1} and (B) 1586 cm^{-1}. Laser wavelength: 647 nm; power: 3mW; lens: 50× long distance objective; acquisition time: 2 s.

which the intensities of SERS spectra are less changed too and the values of RSD of the bands at 1079 and 1586 cm^{-1} are 3.49% and 2.55%, respectively. Moreover, we examined the SERS-activity of the substrates when the samples were kept for weeks, indicating that the enhancement performance was still good (Figure S2). These results indicate that Ag/TiO_2 nanostructures are of stable and uniform substrates for SERS.

It has been proved by previous literature that the large enhancement of the SERS is associated with the existence of hot spots in the SERS substrate.[8,14−16] The local electromagnetic field, which is the main reason of SERS enhancement, turns out to be very strong at "hot spots" in the gaps of adjacent NPs due to the electromagnetic coupling effect.[8,14−16] For our presented substrates, the SEM images in Figure 2 indicate that the TiO_2 NRs are covered by AgNPs with little space among them. The AgNPs are about tens of nanometers in diameter and separated by a distance (d) less than their diameters (D). According to the previous analysis, there is a huge localized EM field in the gap when D is larger than d.[42] Moreover, the TiO_2 NRs chosen in our work were not well perpendicular to the glass surface. Most of them were slightly tangled and close to small bundles. This morphology facilitated the approaching between AgNPs on different NRs and more "hot spots" could be formed. From SEM images we can deduce that hot spots are created from two main levels. The first is due to AgNPs on the single NR with small interparticle distance. The second is due to the crossing and contact between two or more TiO_2 NRs. It is clear that aggregated TiO_2 NRs decreased the distance of AgNPs coated on them. This morphology brought in more hot spots, which was responsible for huge Raman signal enhancement. Compared to 2D substrates, the 3D substrates have another distinct superiority, which is that they have more AgNPs in the probing volume, indicating additional enhancement. Comparing the distribution of AgNPs (Figure 2) and the corresponding SERS spectra (Figure 4), obvious evidence can be found that the Raman signal intensities of PMBA increased with the AgNPs concentration increasing. The results are in agreement with previous studies on SERS-activity of metal NPs-modified nanorod substrates.[23−28]

To clarify the SERS-activity of Ag/TiO_2 structure, we carry out an FDTD simulation, which has been widely applied to describe the electromagnetic field around AgNPs. The result shows that the "hot spots" are mainly located in the gap region between AgNPs adsorbed on the adjacent two rods, and others located between particles adsorbed on the same rod, which is in good accordance with the experimental results (Figure S3). These two kinds of hot spots contribute to the huge enhancement effect of the substrate (details in Supporting Information).

Application for Ultrasensitive MG Detection. MG is a kind of triphenylmethane dye that has been widely used around the world as fungicide, ectoparasiticide, and antiseptic in aquaculture because of its effectiveness against fungal and parasite infections in fish. But it is mutagenic and teratogenic and even carcinogenic to humans, and its usage in aquaculture is banned now. However, the toxic molecule is still used by some unprincipled people in aquaculture because of its low cost and high efficacy. Therefore, it is very important to detect MG in foodstuffs, especially in aquatic products. SERS has been proved as a promising method for rapid and sensitive detection of chemicals and biochemicals. In this work, the Ag/TiO_2 substrate was applied to detect MG. In the experiment, the stock solutions of MG were prepared and diluted in a range of 10^{-7} to 10^{-12} M. The substrates were immersed in the MG solution with concentrations of 10^{-7}, 10^{-8}, 10^{-9}, 10^{-10}, 10^{-11}, and 10^{-12} M for 20 min before SERS measurement, respectively. Figure 7A shows the SERS spectra of MG

dx.doi.org/10.1021/am3004126 | ACS Appl. Mater. Interfaces 2012, 4, 3432−3437

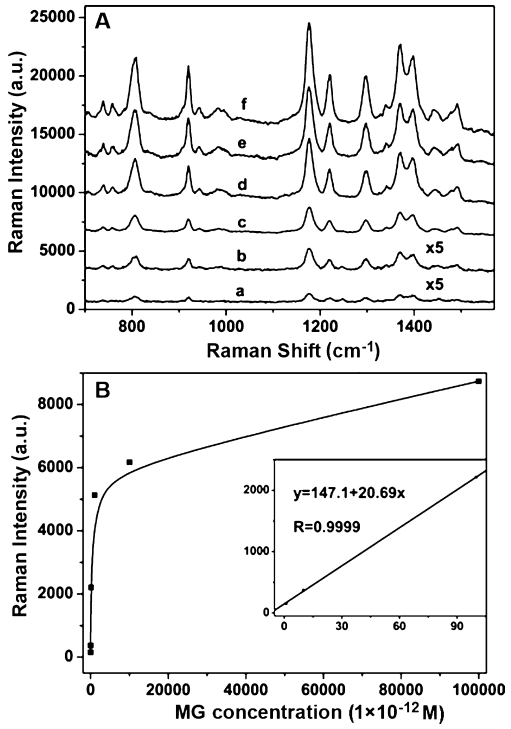

Figure 7. (A) SERS spectra of MG with various concentrations on substrate D (a) 10^{-12}, (b) 10^{-11}, (c) 10^{-10}, (d) 10^{-9}, (e) 10^{-8}, (f) 10^{-7} M. (B) The relationships of peak intensities (bands around 1176 cm^{-1}) and the concentrations of MG. Laser wavelength: 647 nm; power: 3 mW; lens: 50× long distance objective; acquisition time: 2 s, baselines were removed.

adsorbed on substrates with various concentrations. The characteristic bands are distinguishable even with the concentration as low as 10^{-12} M. Band around 1176 cm^{-1}, which is assigned to the in-plane vibrations of ring C−H,[43,44] is selected to depict the relationship between concentration and peak intensity. As shown in Figure 7, the intensities of bands increase monotonously with the concentration of dyes molecule. The concentration was saturated when it reached as high as 10^{-7} M. Considering that the as-prepared nanostructure is of large-scale, high enhancement effect, uniformity, and stability, it can be a potential SERS sensor to detect harmful materials in food.

4. CONCLUSIONS

Wafer-scale 3D nanostructures were fabricated by the modification of TiO_2 NRs scaffold on FTO glass surface using AgNPs in a simple method. The experimental results show that this substrate has high activity, uniformity, and stability. The SEM and TEM study indicated that the density and sizes of AgNPs increased with the deposition times, which induced the decrease of the distance between AgNPs. AgNPs aggregations with small gap distance, so-called hot spots, produce giant Raman enhancement due to strong electromagnetic coupling. There are two kinds of hot spots that both contribute to the huge enhancement effect of the substrate: except hot spots are from AgNPs adsorbed on same rod, more hot spots are from two near crossover rods because of the 3D scaffold configuration, which was reproduced by FDTD simulation results. Because of the above advantages, our presented substrate is considered to be a promising candidate for SERS sensor. Trace of MG could be determined with the detection limit of 1×10^{-12} M when the Ag/TiO_2 nanostructure was used as SERS sensor to detect pollutant species from water. The results indicate that this 3D hybrid nanostructure can be a potential optical sensor used for trace detection in the future.

■ ASSOCIATED CONTENT

Supporting Information

XRD patterns, FDTD simulations, and SERS spectra. This material is available free of charge via the Internet at http://pubs.acs.org.

■ AUTHOR INFORMATION

Corresponding Author

*E-mail: pgyin@buaa.edu.cn (P.-G.Y.); guolin@buaa.edu.cn (L.G.).

Notes

The authors declare no competing financial interest.

■ ACKNOWLEDGMENTS

This work was financially supported by the National Natural Science Foundation of China (20973019 and 51002007) and National Basic Research Program of China (2010CB934700).

■ REFERENCES

(1) Huang, Y. F.; Zhu, H. P.; Liu, G. K.; Wu, D. Y.; Ren, B.; Tian, Z. Q. *J. Am. Chem. Soc.* **2010**, *132*, 9244−9246.
(2) Dasary, S. S. R.; Singh, A. K.; Senapati, D.; Yu, H. T.; Ray, P. C. *J. Am. Chem. Soc.* **2009**, *131*, 13806−13812.
(3) Kaminska, A.; Dziecielewski, I.; Weyher, J. L.; Waluk, J.; Gawinkowski, S.; Sashuk, V.; Fialkowski, M.; Sawicka, M.; Suski, T.; Porowski, S.; Holyst, R. *J. Mater. Chem.* **2011**, *21*, 8662−8669.
(4) Hsiao, W. H.; Chen, H. Y.; Yang, Y. C.; Chen, Y. L.; Lee, C. Y.; Chiu, H. T. *ACS Appl. Mater. Inter.* **2011**, *3*, 3280−3284.
(5) Yang, K. H.; Liu, Y. C.; Yu, C. C. *J. Mater. Chem.* **2008**, *18*, 4849−4855.
(6) Chu, H.; Yang, H. F.; Huan, S. Y.; Shen, G. L.; Yu, Q. *J. Phys. Chem. B* **2006**, *110*, 5490−5497.
(7) Liang, H. Y.; Yang, H. X.; Wang, W. Z.; Li, J. Q.; Xu, H. X. *J. Am. Chem. Soc.* **2009**, *131*, 6068−6069.
(8) Wang, H.; Levin, C. S.; Halas, N. J. *J. Am. Chem. Soc.* **2005**, *127*, 14992−14993.
(9) Zhang, Y. R.; Xu, Y. Z.; Xia, Y.; Huang, W.; Liu, F. A.; Yang, Y. C.; Li, Z. L. *J. Colloid Interface Sci.* **2011**, *359*, 536−541.
(10) Tao, A.; Kim, F.; Hess, C.; Goldberger, J.; He, R. R.; Sun, Y. G.; Xia, Y. N.; Yang, P. D. *Nano Lett.* **2003**, *3*, 1229−1233.
(11) Gunnarsson, L.; Bjerneld, E. J.; Xu, H.; Petronis, S.; Kasemo, B.; Kall, M. *Appl. Phys. Lett.* **2001**, *78*, 802−804.
(12) Hulteen, J. C.; Treichel, D. A.; Smith, M. T.; Duval, M. L.; Jensen, T. R.; Van Duyne, R. P. *J. Phys. Chem. B* **1999**, *103*, 3854−3863.
(13) Cui, B.; Clime, L.; Li, K.; Veres, T. *Nanotechnology* **2008**, *19*, 145302.
(14) Qin, L. D.; Zou, S. L.; Xue, C.; Atkinson, A.; Schatz, G. C.; Mirkin, C. A. *Proc. Natl. Acad. Sci. USA* **2006**, *103*, 13300−13303.
(15) Lee, S. J.; Morrill, A. R.; Moskovits, M. *J. Am. Chem. Soc.* **2006**, *128*, 2200−2201.
(16) Genov, D. A.; Sarychev, A. K.; Shalaev, V. M.; Wei, A. *Nano Lett.* **2004**, *4*, 153−158.
(17) Xu, H.; Bjerneld, E. J.; Käll, M.; Börjesson, L. *Phys. Rev. Lett.* **1999**, *83*, 4357−4360.
(18) Xu, H.; Aizpurua, J.; Käll, M.; Apell, P. *Phys. Rev. E* **2000**, *62*, 4318−4324.
(19) Xu, H.; Käll, M. *Chemphyschem* **2003**, *4*, 1001−1005.
(20) Chan, S.; Kwon, S.; Koo, T. W.; Lee, L. P.; Berlin, A. A. *Adv. Mater.* **2003**, *15*, 1595−1598.

(21) Williamson, T. L.; Guo, X. Y.; Zukoski, A.; Sood, A.; Diaz, D. J.; Bohn, P. W. *J. Phys. Chem. B* **2005**, *109*, 20186−20191.
(22) Ko, H.; Tsukruk, V. V. *Small* **2008**, *4*, 1980−1984.
(23) Galopin, E.; Barbillat, J.; Coffinier, Y.; Szunerits, S.; Patriarche, G.; Boukherroub, R. *ACS Appl. Mater. Inter.* **2009**, *1*, 1396−1403.
(24) Tang, J.; Ou, F. S.; Kuo, H. P.; Hu, M.; Stickle, W. F.; Li, Z. Y.; Williams, R. S. *Appl. Phys. A: Mater. Sci. Process.* **2009**, *96*, 793−797.
(25) Chen, J. N.; Martensson, T.; Dick, K. A.; Deppert, K.; Xu, H. Q.; Samuelson, L.; Xu, H. X. *Nanotechnology* **2008**, *19*, 275712.
(26) Becker, M.; Stelzner, T.; Steinbruck, A.; Berger, A.; Liu, J.; Lerose, D.; Gosele, U.; Christiansen, S. *Chemphyschem* **2009**, *10*, 1219−1224.
(27) Deng, S.; Fan, H. M.; Zhang, X.; Loh, K. P.; Cheng, C. L.; Sow, C. H.; Foo, Y. L. *Nanotechnology* **2009**, *20*, 175705.
(28) Sakano, T.; Tanaka, Y.; Nishimura, R.; Nedyalkov, N. N.; Atanasov, P. A.; Saiki, T.; Obara, M. *J. Phys. D: Appl. Phys.* **2008**, *41*, 235304.
(29) Li, X. H.; Chen, G. Y.; Yang, L. B.; Jin, Z.; Liu, J. H. *Adv. Funct. Mater.* **2010**, *20*, 2815−2824.
(30) Sinha, G.; Depero, L. E.; Alessandri, I. *ACS Appl. Mater. Inter.* **2011**, *3*, 2557−2563.
(31) Liu, B.; Aydil, E. S. *J. Am. Chem. Soc.* **2009**, *131*, 3985−3990.
(32) Wang, H.; Bai, Y. S.; Zhang, H.; Zhang, Z. H.; Li, J. H.; Guo, L. *J. Phys. Chem. C* **2010**, *114*, 16451−16455.
(33) Wang, H.; Bai, Y. S.; Wu, Q.; Zhou, W.; Zhang, H.; Li, J. H.; Guo, L. *Phys. Chem. Chem. Phys.* **2011**, *13*, 7008−7013.
(34) Zhang, H.; Lv, X. J.; Li, Y. M.; Wang, Y.; Li, J. H. *ACS Nano* **2010**, *4*, 380−386.
(35) Li, X. L.; Hu, H. L.; Li, D. H.; Shen, Z. X.; Xiong, Q. H.; Li, S. Z.; Fan, H. J. *ACS Appl. Mater. Inter.* **2012**, *4*, 2180−2185.
(36) Chen, Y. J.; Tian, G. H.; Pan, K.; Tian, C. G.; Zhou, J.; Zhou, W.; Ren, Z. Y.; Fu, H. G. *Dalton Trans.* **2012**, *41*, 1020−1026.
(37) Jain, P. K.; Huang, X. H.; El-Sayed, I. H.; El-Sayed, M. A. *Acc. Chem. Res.* **2008**, *41*, 1578−1586.
(38) Orendorff, C. J.; Gole, A.; Sau, T. K.; Murphy, C. J. *Anal. Chem.* **2005**, *77*, 3261−3266.
(39) Yin, P. G.; You, T. T.; Tan, E. Z.; Li, J.; Lang, X. F.; Jiang, L.; Guo, L. *J. Phys. Chem. C* **2011**, *115*, 18061−18069.
(40) He, P.; Liu, H. T.; Li, Z. Y.; Liu, Y.; Xu, X. D.; Li, J. H. *Langmuir* **2004**, *20*, 10260−10267.
(41) Ji, N.; Ruan, W. D.; Wang, C. X.; Lu, Z. C.; Zhao, B. *Langmuir* **2009**, *25*, 11869−11873.
(42) Lee, S. J.; Guan, Z. Q.; Xu, H. X.; Moskovits, M. *J. Phys. Chem. C* **2007**, *111*, 17985−17988.
(43) Canamares, M. V.; Chenal, C.; Birke, R. L.; Lombardi, J. R. *J. Phys. Chem. C* **2008**, *112*, 20295−20300.
(44) He, L. L.; Kim, N. J.; Li, H.; Hu, Z. Q.; Lin, M. S. *J. Agric. Food Chem.* **2008**, *56*, 9843−9847.